Tunnelling and Underground Space Technology 47 (2015) 114–122

Contents lists available at ScienceDirect

Tunnelling and Underground Space Technology

journal homepage: www.elsevier.com/locate/tust

freepaper.me FREE paper

Numerical study of the depth and cross-sectional shape of tunnel under surface explosion

Behnam Mobaraki [a], Mohammad Vaghefi [b,*]

[a] Islamic Azad University of Bushehr, Iran
[b] Persian Gulf University, Bushehr, Iran

ARTICLE INFO

Article history:
Received 24 April 2014
Received in revised form 10 October 2014
Accepted 4 January 2015
Available online 29 January 2015

Keywords:
Dynamic response
Numerical simulation
Kobe metro
Surface explosion
Buried structure

ABSTRACT

Recently, blasting loads have come into consideration because of the large number of intentional or unintentional events that affected important structures around the world, obviously indicating that the topic is relevant for purposes of structural design and reliability analysis. This paper has evaluated the dynamic responses of buried tunnel in depths of 3.5, 7, 10.5 and 14 m for surface detonation of 1000 kg TNT charge in a surrounding sandy soil. The Kobe box shape subway tunnel was used as an example to evaluate and compare with semi ellipse, circular and horseshoe shape tunnel. The finite element software LS-DYNA has been used to model and to analyze the outcome of this project, specifically to be modeled in the area of the second interaction due to explosion. The results indicate that the circular and horseshoe tunnels are less resistant to demolition than the box shape tunnel however the semi ellipse tunnel is more resistant than the box shape tunnel.

© 2015 Elsevier Ltd. All rights reserved.

1. Introduction

In recent years the worldwide terrorism attacks are becoming intensive and more frequent. Vehicle bomb is the main way that terrorists put their plans into action due to its enormous charge power and acute demolition. Subway is one of the public places that might be affected by such events. One aspect in the protection of such structures is the accurate prediction of the blast loadings on structural components using analytical or experimental study or advanced numerical tools taking into account the complexity of the structure. Therefore it is necessary to estimate the dynamic behaviors of underground structures subject to blasting vibration to ensure the safety of these structures.

The influence of blasting vibration on underground structures have been studied by many scholars using field experiments. For example, the US Army Corps of Engineers performed some huge-scale explosion tests during the years 1948–1952 near unlined tunnels in sandstone (Hendron, 1977). In this report, the damage was classified into four groups: intermittent failure, local failure, general failure, and tight closure. Table 1 shows that tunnel peak particle velocity (PPV) damage criterion for different damage zones. Kendorski et al. (1973) gave an account of his researches that cracks in the shotcrete liner of tunnels occur when the PPV exceeds roughly 1.22 m/s. Cheesman et al. (2006) performed a coupled Eulerian–Lagrangian analysis to study the blast output of explosives buried in saturated sand. The explosive charge size, its depth of burial, the target stand-off, the distance and the dimensions of the target were varied and the accuracy of the numerical simulations where compared with the experimental observations. Nakano et al. (1993) informed that the shotcrete cracking caused by an adjacent tunnel blast happened when the PPV reached 0.7 m/s. Most experimental formulae available in the literature usually work well for certain specific types of rock mass and do not include the effect of loading density, the chamber geometry and the explosive distribution.

With the quick increase of computer technology and jutting numerical methods, more detail and authentic prediction of underground structure damage under blast loading through numerical simulation have become available. Different numerical methods have been suggested to assess the rock mass or the tunnel damage induced by the blast loading. For example Wang and Lu (2003) and Wang et al. (2004) formulated a numerical three-phase soil model which is capable of simulating explosion and blast wave propagation in soils. Using this model, Lu et al. (2005) and Wang et al. (2005), performed fully coupled numerical model simulations of the response of a buried structures under underground explosions. The SPH (smooth particle hydrodynamics) technique was used to model the explosive charge, while the normal FEM is used to model

* Corresponding author.
E-mail addresses: Behnam.Mobaraki@yahoo.com (B. Mobaraki), Vaghefi52@gmail.com (M. Vaghefi).

http://dx.doi.org/10.1016/j.tust.2015.01.003
0886-7798/© 2015 Elsevier Ltd. All rights reserved.

Table 1
UET tests, sandstone (Hendron, 1977).

Damage zone	Damage	PPV (m/s)
1	Tight closure	NA
2	General failure	12
3	Local failure	4
4	Intermittent failure	0.9–1.8

the remaining soil region and the buried structure. A good agreement of numerical results with empirical predictions was found in both papers. Luo et al. (2007) analyzed the dynamic responses of the tunnel for surface explosion of 100 and 300 kg TNT charge, respectively, according to features of Nanjing metro tunnel in sandy soil.

Along with the undertaken researches, this research is carried out with the finite element software LS-DYNA for the dynamic response of the Kobe box shape subway tunnel (in a sandy soil) in depths of 3.5, 7, 10.5 and 14 m, affected by surface explosion of 1000 kg TNT charge. In order to ensure the analysis accuracy, the numerical results have been compared with the analytical formulas of the US Army Corps of Engineering Manual (TM5-855-1) (Nagy et al., 2010).

Eventually based on the tunnel vertical PPV criterion (Li et al., 2013), the above comparisons have been carried out for the circular, semi ellipse and horseshoe tunnel with the same area and condition to the box shape tunnel as shown in Fig. 1.

2. Numerical model

2.1. Background and finite element model

The project of the Kobe metro is considered in this paper. The tunnel is box shape, with size of 9 m × 7.17 m (Kongai et al., 2001). Moreover, according to the typical Kobe stratigraphic distribution, the soil layer around the tunnel consists of gravel, clay and sand but it is assumed that the entire soil layer has the same parameters as the sand for computational simplicity.

The affected region of detonation (1000 kg TNT) in the soil and tunnel, was studied by varying the length of tunnel from 10 m to 30 m in the numerical simulation. It was found that over 25 m, varying the tunnel length causes only insignificant changes in the blast load on the tunnel. So only the results with the tunnel length of 25 m are presented in the paper. The tunnel is centered under the explosive charge and only a quarter of field with the size of 25 m × 25 m × 30 m is modeled due to the symmetry about the YZ and YX planes as shown in Fig. 2. Furthermore, the transitional displacement of the nodes normal to the symmetry planes (YZ and YX planes) is constrained. The non-reflection-boundaries are applied to the two lateral surfaces and the bottom surface in order to minimize the stress wave reflection at these computational boundaries, and the free boundary condition is used for upper surface (Wei et al., 2009).

In the symmetric model with box shape tunnel, the model consist of 156,570 elements, with 128,720 elements to model the soil, 25,500 elements to model the air, 2346 elements to model the tunnel and 4 elements to model the TNT.

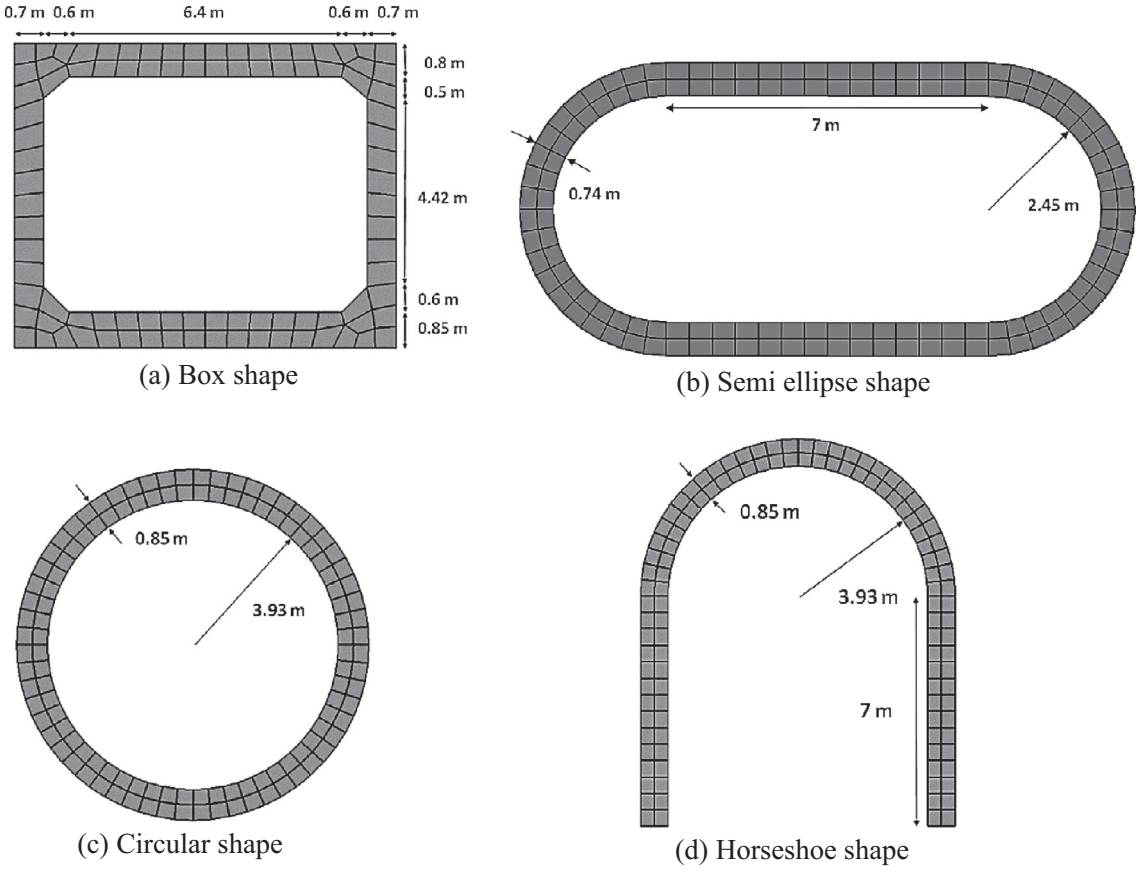

Fig. 1. Tunnels dimensions.

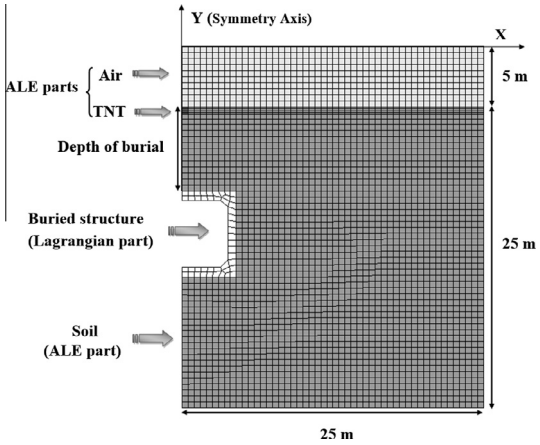

Fig. 2. The finite element model.

Table 2
Material model and EOS parameters of TNT.

ρ (kg/m^3)	v_D (m/s)	P_{cut} (Mpa)	A (Mpa)	B (Mpa)
1630	6930	2.1×10^4	3.738×10^5	3.747×10^3
R_1	R_2	ω	V_0	E_0 (Mpa)
4.15	0.9	0.35	1	6×10^3

Table 3
Material model and EOS parameters of air.

ρ (kg/m^3)	C_0	C_1	C_2	C_3	C_4	C_5	C_6	E_0 (Mpa)	V_0
1.29	0	0	0	0	0.4	0.4	0	0.25	1

Table 4
Triaxial hydrostatic compression data for sandy soil.

True volumetric strain	0.05	0.1	0.15	0.2	0.25	0.3	0.33
Pressure (MPa)	0.02	0.05	0.07	0.12	0.2	0.34	0.5

2.2. Material model

A summary description of the material models assigned for the tunnel, TNT charge, air and soil is presented in this section. In the finite element model, SOLID 164 is adopted for the 3D explicit analysis (Xu et al., 2011). This element is used in explicit dynamic analysis and is only defined by eight nodes having the following degrees of freedom at each node: Translations, velocities and accelerations in the nodal X, Y and Z directions (ANSYS User Manual v12, 2009).

Mesh sensitivity of the three-dimensional results were assessed. Four meshes, with element sizes of 25 cm, 50 cm, 75 cm and 100 cm, were used for the three-dimensional analyzes. The results corresponding to the meshes of 25 cm and 50 cm were very coincident. It can be concluded that the mesh of 50 cm gives an accurate solution to the problem.

2.2.1. TNT

The TNT charge is modeled by the material type 8 of LSDYNA (*MAT_HIGH_EXPLOSIVE_BURN) (Cheng et al., 2013). The Jones–Wilkens–Lee (JWL) equation of state (EOS) is used to model the pressure released by chemical energy during the explosion and it has been widely used in engineering calculations. The JWL EOS can be written in the following form:

Table 5
Material model and parameters of soil.

ρ (kg/m^3)	G (MPa)	K_u (MPa)	a_0	a_1	a_2	P_{cut} (MPa)
1255	1.7240	5.5160	0	0	0.8702	0

Table 6
Material model and parameters of tunnel.

ρ (kg/m^3)	E (GPa)	υ	σ_y (MPa)	E_{tan} (MPa)	β	ε_f
2650	39.1	0.25	100	4000	0.5	0.8

$$P = A\left(1 - \frac{\omega}{R_1 V}\right)e^{-R_1 V} + B\left(1 - \frac{\omega}{R_2 V}\right)e^{-R_2 V} + \frac{\omega E_0}{V} \quad (1)$$

where P is the detonation pressure, E is the internal energy per unit volume, V is the relative volume of detonation product, A, B, R_1, R_2 and ω are material constants (LSTC, 2007). Table 2 gives the parameters used in TNT (AUTODYN user manual v12, 2009).

2.2.2. Air

The air is modeled by the material type 9 of LS-DYNA (*MAT_NULL) with linear polynomial EOS (Cheng et al., 2013), which is linear in internal energy per unit volume, E, and pressure P, and is given by

$$P = C_0 + C_1\mu + C_2\mu^2 + C_3\mu^3 + (C_4 + C_5\mu + C_6\mu^2)E_0 \quad (2)$$

$$\mu = \rho/\rho_0 - 1 \quad (3)$$

where C_0, C_1, C_2, C_3, C_4, C_5 and C_6 are constant, ρ/ρ_0 is the ratio of current density and E_0 is the initial internal energy per volume (LSTC, 2007). Table 3 gives the parameters used in the air (AUTODYN user manual v12, 2009).

2.2.3. Soil

Soil is modeled by the material type 5 of LS-DYNA (*MAT_SOIL_AND_FOAM) (Yang et al., 2010) put forward by Krieg (1972). The material properties of the soil were reported by Foster et al. (2005) and the properties were evaluated from National Soil Dynamics and Auburn University (NSDL-AU) soil compaction model components (Bailey and Johnson, 1989). Tables 4 and 5 give the parameters used in Soil (Kulak and Bojanowski, 2011).

where ρ is mass density, G is shear modulus, K_u is bulk modulus at unloading path, a_0, a_1 and a_2 are yield function constants and P_{cut} is pressure cutoff for tensile fracture (LSTC, 2007).

2.2.4. Tunnel

The tunnel is modeled by material type 3 of LS-DYNA (*MAT_PLASTIC_KINEMATIC) (Yang et al., 2010). The steel bar and the concrete are regarded as a whole according to the principle of equivalent stiffness EI. The tunnel liner was made of C_{50} concrete.

where ρ is mass density, E is Young modulus, υ is Poisson ratio, σ_y is yield stress, E_{tan} is tangent modulus, β is hardening parameter, ε_f is failure strain for eroding elements (LSTC, 2007). Table 6 gives parameters used in the tunnel.

2.3. Numerical solver

Different solvers are available in a finite element software LS-DYNA to model various materials and conditions. Common solvers available in LS-DYNA are Lagrange, Euler and Arbitrary Lagrange Euler (ALE). The Lagrange formulation more accurately determines the positions of material interfaces and facilitates the inclusion of

freepaper.me FREE paper

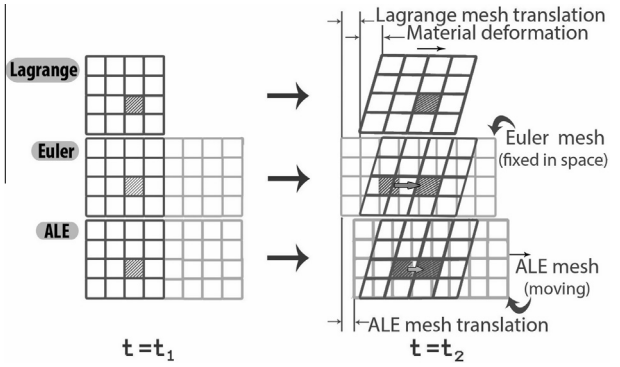

Fig. 3. Lagrangian, Eulerian and ALE meshes and elements motion.

slip, slide or friction at interfaces. Since the mesh is embedded in the material, the motion of the material is inferred from the motion of the mesh. The Euler formulation is more robust, since the mesh remains unchanged and no tangling occurs. The ALE method combines the advantages of the two approaches while limiting the disadvantages such as diffusion. As shown in Fig. 3, in the ALE formulation the mesh may remains fixed, as in an Euler formulation, move with the material, as in a Lagrange formulation, or move in a manner between these two formulations (Cheng et al., 2013).

The default constant stress solid formulation (ELFORM = 1) is used for the Tunnel. The multi material ALE solver (ELFORM = 11) is used for the TNT, air and soil to eliminate the distortion of the mesh under high deformation and specified as multi material using LS-DYNA multi material capabilities (*ALE_MULTI_MATERIAL_GROUP). (Jayasinghe et al., 2013). *CONSTRAINED_LAGRANGE_IN_SOLID command is applied to provides the coupling mechanism for modeling soil-structure interaction. This option may be used to allow the coupling between the edge of a solid part and one or more ALE multi-material groups (LSTC, 2007).

3. Numerical results and discussions

Considering the tunnel depths and Geometry, the following calculation cases are performed in Table 7.

3.1. Comparison between numerical and analytical results by the manual TM5-855-1

The US Army Corps of Engineers Manual (TM5-855-1) has been used to predict the peak values of pressure at different depths of the soil in case 0. The following equation provided in the manual TM5-855-1 (1986).

$$P_p = 0.407 f \rho_c \left(\frac{R}{w^{1/3}}\right)^{-n} \quad (4)$$

where P_p is the peak pressure, f is a coupling factor for the explosion, which is dependent of the scaled depth of the explosion and is given by $\left(\frac{d}{w^{1/3}}\right)$, d is the depth of the centroid of the explosive charge, w is the charge weight, ρ_c is the acoustic impedance, R is the distance from the source and n is an attenuation coefficient. Based on the seismic velocity of the sandy soil, the soil in this paper is described as the type 4 in the manual (TM5-855-1) as shown in Table 8.

Using the parameters of the soil type 4 in Table 8, and f is equal to 0.4 (TM 5-855-1, 1986), one can calculate peak pressure at different depths of the soil. The peak pressure at depths of 1–10 m of soil right below the explosion is calculated. Fig. 4 illustrate a comparison between numerical results and analytical result obtained from design manual TM5-855-1, against scaled distance ($d/w^{1/3}$). As shown in Fig. 4, the reduction of peak pressure increases, with increasing distance from detonation. The results obtained from numerical analyzes are considered in good agreement with those derived from TM5-855-1 design manual.

Fig. 5 describes the compressive waves in the soil at different depths below the explosion center. For example, the peak pressure at depths 4, 5, 6, 7 and 8 m are 2.74, 1.48, 0.65, 0.21 and 0.11 MPa. Compared with depth of 4 m, they decrease by 46%, 76%, 92% and 96% respectively.

From Fig. 4 it is obvious that the outcomes of the manual (TM5-855-1) are higher than the numerically obtained results, which has been provided to ensure the regulation.

In the year 1967 the Alekseenko test (Henrych and Major, 1979) showed that, if the upper surface of the charge was at the same level as the ground surface, the proportion of the energy would be absorbed by the air, same as the case in this paper. This conclusion can elucidate the difference between numerical and analytical results.

3.2. Structure response

3.2.1. The wall behavior

A number of target points on the Kobe tunnel wall are selected to record the tunnel response. As shown in Fig. 6a. these points are: the wall corner point (1), the wall quarter span point (2) and the wall center point (3).

Table 7
Calculation cases.

Geometry	Box shape				Horseshoe shape				Semi ellipse shape				Circular shape				Free field
Case	1	2	3	4	1	2	3	4	1	2	3	4	1	2	3	4	0
Depth (m)	3.5	7	10.5	14	3.5	7	10.5	14	3.5	7	10.5	14	3.5	7	10.5	14	–
TNT (kg)	250																

Table 8
soil properties for calculating ground shock parameters (TM 5-855-1, 1986).

Soil type	Density, ρ (kg/m^3)	Seismic velocity, c (m/s)	Acoustic impedance, $\rho_c\left(10^6 Pa.\frac{s}{m}\right)$	Attenuation coefficient, n
(1) Heavy saturated clays and clay shale	1920–2080	>1524	33.9–40.68	1.5
(2) Saturated sandy clays and sands with air voids <1%	1760–1984	1524	29.38	2.25–2.5
(3) Dense sand with high relative density	1744	487.68	9.944	2.5
Wet sandy clay with air voids >4%	1920–2000	548.64	10.848	2.5
(4) Sandy loam, loess, dry sands and backfills	1984	304.8	4.972	2.75
(5) Loose, dry sands and gravels with low relative density	1440–1600	182.88	2.712	3–3.25

freepaper.me FREE paper

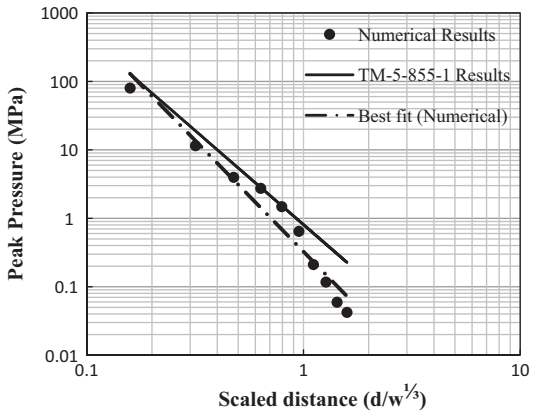

Fig. 4. Comparison between numerical and analytical results.

Fig. 7 presents the time histories of the lateral deformation of the tunnel wall for the target points 1, 2 and 3 in case 1, 2, 3 and 4 (Zhang et al., 2014). It demonstrates that the wall has suffered permanent deformation under the surface explosion and the maximum residual deformation, occurs at point 3 located at the wall center. The difference in the behavior of the tunnel at these three points is owing to the variation of the pressure generated by the blast loads as well as due to the nonlinearity of the concrete. These residual deflections indicate the occurrence of plastic deformation of the tunnel under the effect of the blast loads.

3.2.2. The roof behavior

To estimate the dynamic responses of the tunnel caused by blasting vibration (Lu et al., 2011), we selected the element right below the explosion center at the roof center point (4) and the roof corner point (5) as these are the most critical parts of the tunnel from a design point of view shown in Fig. 6b.

As shown in Fig. 8 the vertical PPVs of point 4 and 5 for box shape tunnel case 1 are 0.358 m/s and 0.169 m/s respectively. It can be seen that roof center element has larger vertical PPV (52.8%) than roof corner element and it is higher than 0.9 m/s by detonation of 1000 kg TNT.

Also in Box shape tunnel case 3 the vertical PPV of point 5 (0.0188 m/s) is 38.8% of that at point 4 (0.0484 m/s). Hence the roof center seems more vulnerable compared to the roof corner. Figs. 8 and 9 indicate that when the tunnel depth increases 7 m, the vertical PPVs of the roof center point (4) and the roof corner point (5) decrease by 86.5% and 88.9% consecutively.

It can been seen that the second peak for Point A is higher than the 1st peak for point. The reason can explain by its close distance away from surface zone and explosion. The first peak value is caused by the ground wave and the second is caused by the air shock wave and the reflected wave at the soil interface (Henrych and Major, 1979). As shown in Figs. 8 and 9 the PPV are different between point A and B. The reduction trends of vibration velocity are also different for point A and B. This difference indicate that Point A receives more energy from the blasting wave than Point B.

Table 9 presents the vertical PPVs of points 4 and 5 for all cases, which can assess the critical depth for all tunnel cases. Fig. 10 indicates the trend of effective stress of point 4 and 5 for box shape tunnel case 3. As shown the effective stress of point 5 attenuates notably more slowly and its peak effective stress (0.858 MPa) is smaller (62.7%) than that at point 4 (2.3 MPa). This amount of difference is almost equal to their amount of difference in the vertical PPV.

3.3. Safety evaluation of tunnels

It is too difficult to obtain generally accepted damage criterion since it involves many factors. Generally speaking, the damage

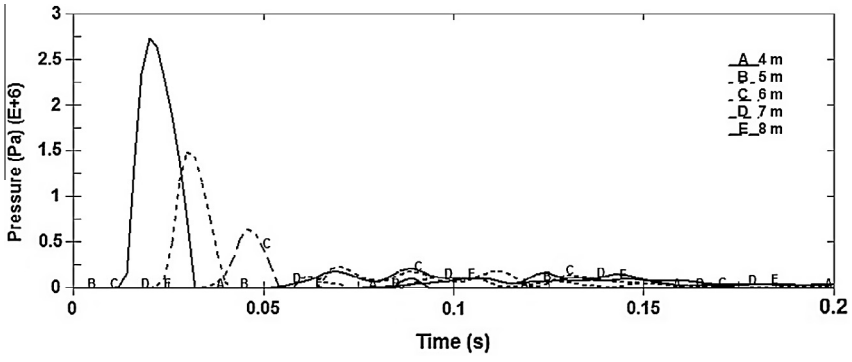

Fig. 5. Compressive waves in the soil at different depths (case 0).

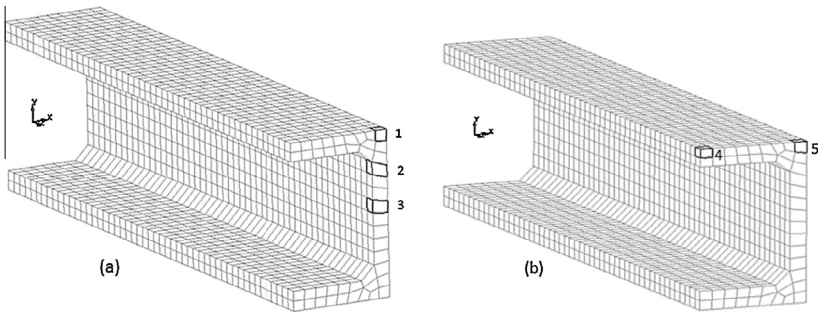

Fig. 6. Evaluation points of the Kobe tunnel.

freepaper.me FREE paper

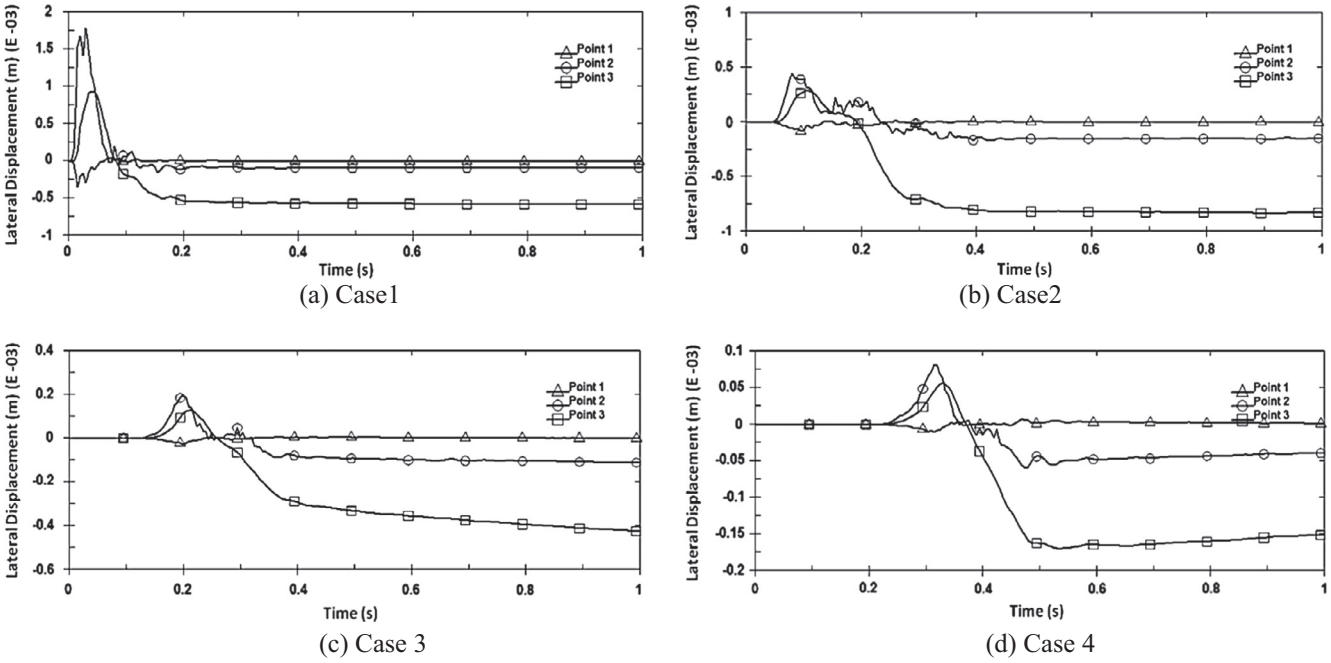

Fig. 7. Lateral displacement of the Kobe tunnel wall.

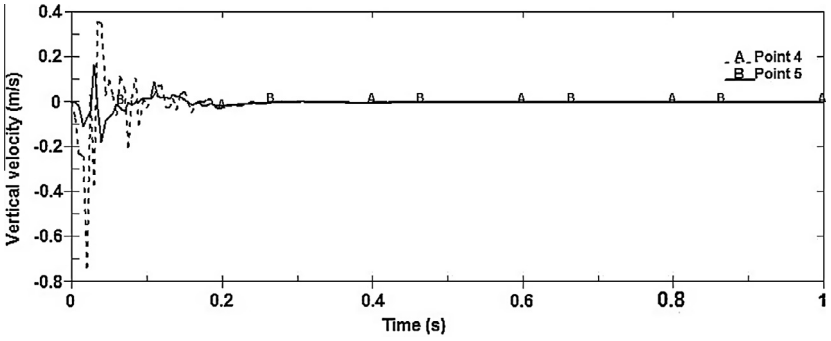

Fig. 8. Vertical velocities of point 4 and 5 (Box shape case 1).

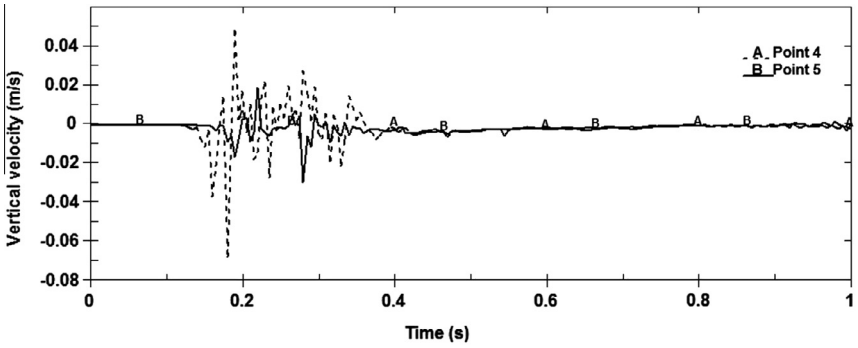

Fig. 9. Vertical velocities of point 4 and 5 (Box shape case 3).

degree from an explosion depends on many parameters that include the amount of explosive, shape of the load, the explosion depth, type of the soil and properties.

There are some empirical PPV criteria to evaluate the possible failure of underground structure. For example Hendron (1977) summarized the large explosion tests carried out by US Army Corps

Table 9
Peak particle velocities of point 4 and 5.

Geometry	TNT (kg)	Case	Depth (m)	Point 4 Vertical PPV (m/s)	Point 5	Difference (%)
Box shape	250	1	3.5	0.358	0.169	52.8
		2	7	0.323	0.0211	93.5
		3	10.5	0.0484	0.0188	61.2
		4	14	0.0123	0.00486	60.5
Horseshoe shape		1	3.5	0.81	0.107	86.8
		2	7	0.314	0.0265	91.6
		3	10.5	0.0495	0.0137	72.3
		4	14	0.0481	0.00703	85.4
Semi ellipse shape		1	3.5	0.198	0.0988	50.1
		2	7	0.174	0.067	61.5
		3	10.5	0.0396	0.0236	40.4
		4	14	0.0155	0.0084	45.8
Circular shape		1	3.5	0.773	0.0918	88.1
		2	7	0.101	0.0309	69.4
		3	10.5	0.0713	0.0178	75
		4	14	0.0336	0.00237	93.9

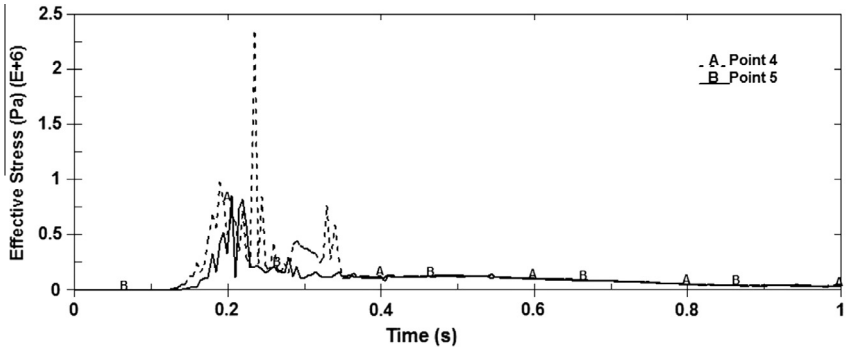

Fig. 10. Effective stresses of point 4 and 5 (Box shape case 3).

of Engineers during the years 1948–1952 near unlined tunnels in sandstone. It was found that, on average, no rock fall occurred in tunnels until the PPV exceeded 0.9 m/s. Fig. 11 shows the vertical PPVs for all cases which can compare with the tunnel PPV damage criterion presents in Table 1.

As shown in Fig. 11, PPVs for different shapes of tunnel are different because the soil-structure interaction for different shapes of underground structures are different. One of the main reasons, is that the length of contact zone between soil and buried structure varies for different tunnel shapes. For example semi ellipse tunnel has the maximum length of contact with soil compared with the other three tunnels, so it suffers the least PPV. Indeed extension the length of contact zone between soil and buried structure, causes to increase the rigidity and stability of the structure.

Fig. 11 demonstrates that the maximum vertical PPV of the Kobe box shape subway tunnel occurring at case 1 (0.54 m/s), and the rest at cases 2–3–4 are 0.32 m/s, 0.066 m/s, 0.033 m/s respectively. Compared with case 1, they decrease by 40.7%, 87.7% and 93.8% respectively. According to the failure criterion proposed in Table 1, the Kobe tunnel will fail at depths of 3.5 and 7 m by detonation of 1000 kg TNT. Based on the observations the circular and horseshoe tunnels are less resistant to demolition than box shape tunnel however the semi ellipse tunnel is more resistant than the Kobe box shape subway tunnel. The vertical PPVs of semi ellipse tunnel at cases 1–2–3–4 are 0.303 m/s, 0.211 m/s, 0.057 m/s and 0.025 m/s respectively. Compared with the rectangular tunnel, they decrease by 43.9%, 34.4%, 13.6% and 24.2% respectively.

Fig. 12(a) and (b) indicate the peak effective stresses and the peak pressures for roof middle elements of semi ellipse tunnel case 4 along point 4 (z direction) at distances of 2.5 m.

Generally speaking, the peak pressure and the peak effective stress soar ranging from 0 to 2 m and fall dramatically between distances 2 to 5 m from the blast center. After initial shock pulse a longer period of fluctuations happens, indicating the involvement of the tunnel response. It is evident that distances 0–2 m from the blast center is more vulnerable compared to the distances 2–25 m. It shows that the tunnel response decreases with the increase of

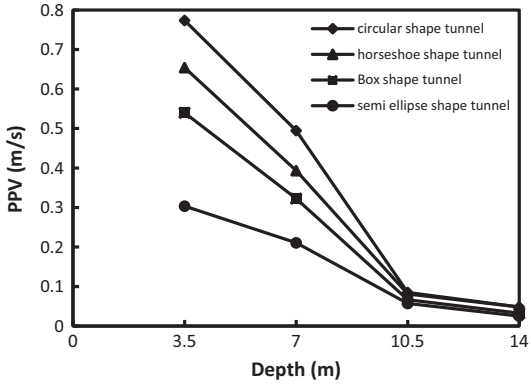

Fig. 11. The vertical PPVs for all cases.

freepaper.me FREE paper

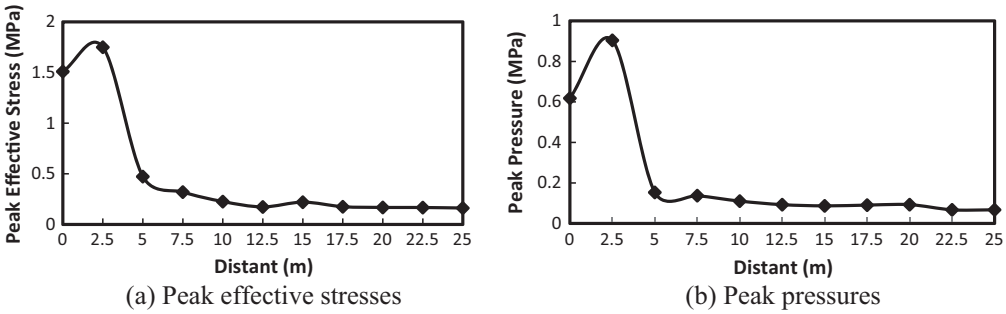

Fig. 12. The variations of the peak effective stresses and the peak pressures along z direction for semi ellipse tunnel case 4.

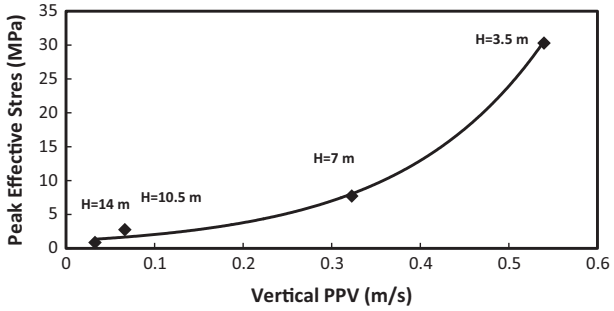

Fig. 13. The exponential relationship of the peak effective stresses and vertical PPVs in Kobe tunnel.

distance from the TNT charge, due to the reduction of the compressive waves in the soil.

The relationship model of the peak effective stresses (PES) and the vertical PPVs in box shape tunnel is specified and shown in Fig. 13 (Jiang and Zhou, 2012). The relationship model established from Fig. 13 is as follows:

$$PES = 1.108\exp(6.145PPV) \quad (R^2 = 0.933)$$

4. Conclusions

(a) The peak pressures at depths of 4, 5, 6, 7 and 8 mr of the soil calculated by the numerical method and the analytical formula obtained from the manual TM5-855-1 and their differences are 2.8%, 3.2%, 29%, 65% and 73% respectively.

(b) The lateral displacement of the Kobe tunnel wall measured for 3 points: the wall corner, at the joint of wall and roof, the wall quarter span and the wall center. The maximum residual deformation happened at the wall center. The difference in the behavior of the tunnel at these points is stems from the variation of the pressure generated by blast loads also due to the nonlinearity of the concrete.

(c) The vertical PPVs of the roof center elements and the roof corner elements for the Kobe tunnel case 1 measured. It indicated that the vertical PPV of the roof corner element is 47.2% of that at roof center element. it means that the roof center is more critical than roof corner when the tunnel is centered under the explosive charge.

(d) It illustrated that distances 0–2 m from the blast center is more vulnerable compared to the distances 2–25 m. It means that the tunnel response decreases with the increase of distance from the blast center, due to the diminution of the compressive waves in the soil.

(e) It is evident that the circular and horseshoe tunnels are less resistant to demolition than box shape tunnel however the semi ellipse tunnel is more resistant than the Kobe box shape subway tunnel.

References

ANSYS, 2009. User Manual Version 12.
ANSYS Inc. AUTODYN, 2009. User Manual Version 12.
Bailey, A.C., Johnson, C.E., 1989. A soil compaction model for cylindrical stress states. Trans. ASABE 32 (3), 822–825.
Cheesman, B.A., Wolf, S., Yen, C.F., Skaggs, R., 2006. Blast simulation of explosive buried in saturated sand. Fragblast 10 (1), 1–8.
Cheng, D., Hung, C., Pi, S., 2013. Numerical simulation of near-field explosion. J. Appl. Sci. Eng. 16 (1), 61–67.
Foster, W.A., Johnson, C.E., Chiroux, R.C., Way, T.R., 2005. Finite element simulation of cone penetration. Appl. Math. Comput. 162, 735–749.
Hendron, A.J., 1977. Engineering of rock blasting on civil projects. In: Hall, W.J. (Ed.), Structural and Geotechnical echanics, A Volume Honoring NM Newmark. Prentice Hall, New Jersey.
Henrych, J., Major, R., 1979. The Dynamics of Explosion and its Use. Elsevier, Amsterdam.
Jayasinghe, L.B., Thambirtnam, D.P., Perera, N., Jayasooriya, J.H.A.R., 2013. Computer simulation of underground blast response of pile in saturated soil. Comput. Struct. 120, 86–95.
Jiang, N., Zhou, C., 2012. Blasting vibration safety criterion for a tunnel linear structure. Tunnel. Underground Space Technol. 32, 52–57.
Kendorski, F.S., Jude, C.V., Duncan, W.M., 1973. Effect of blasting on shotcrete drift linings. Min. Eng. 25 (12), 38–41.
Kongai, K., Kamiya, H., Nishiyama, S., 2001. Deformation buildup in soils during the Kobe earthquake of 1995. Seism. Fault-induced Failures, 81–90.
Krieg, R.D., 1972. A Simple Constitutive Description for Cellular Concrete. Sandia National Laboratories.
Kulak, R.F., Bojanowski, C., 2011. Modeling of cone penetration test using SPH and MM-ALE approaches. In: 8th European LS-DYNA User Conference, Strasbourg, pp. 1–10.
Li, J.C., Li, H.B., Ma, G.W., Zhou, Y.X., 2013. Assessment of underground tunnel stability to adjacent tunnel explosion. Tunnel. Underground Space Technol. 35, 227–234.
LSTC, 2007. LS-DYNA Keyword User's Manual. Livermore Software Technology Corporation.
Lu, Y., Wang, Z., Chong, K., 2005. A comparative study of buried structure in soil subjected to blast load using 2D and 3D numerical simulations. Soil Dyn. Earthquake Eng. 25, 275–288.
Lu, W., Yang, J., Chen, M., Zhou, C., 2011. An Equivalent method for blasting vibration simulation. Simul. Model. Pract. Theory 19, 2050–2062.
Luo, K.S., Wang, Y., Zhang, Y.T., Huang, L.K., 2007. Numerical simulation of section subway tunnel under surface explosion. J. PLA Univ. Sci. Technol. (Nat. Sci. Ed.). 8 (6), 674–679.
Nagy, N., Mohamed, M., Boot, J.C., 2010. Nonlinear numerical modeling for the effects of surface explosions on buried reinforced concrete structures. Geomech. Eng. 2 (1), 1–18.
Nakano, K., Okada, S., Furukawa, K., Nakagawa, K., 1993. Vibration and cracking of tunnel lining due to adjacent blasting. In: Rombun-Hokokushu, D.G. (Ed.), Proceedings of the Japan Society of Civil Engineers, pp. 53–62 (in Japanese).
TM 5-855-1, 1986. Fundamental of Protective Design for Conventional Weapons. Vicksburg, US, US Army Engineers Waterways Experimental Station.
Wang, Z., Lu, Y., 2003. Numerical analysis on dynamic deformation mechanism of soils under blast loading. Soil Dyn. Earthquake Eng. 23, 705–714.
Wang, Z., Hao, H., Lu, Y., 2004. A three-phase soil model for simulating stress wave propagation due to blast loading. Numer. Anal. Meth. Geomech. 28 (1), 33–56.

freepaper.me FREE paper

Wang, Z., Lu, Y., Hao, H., Chong, K., 2005. A full coupled numerical analysis approach for buried structures subjected to surface blast. Comput. Struct. 83, 339–356.
Wei, X.Y., Zhao, Z.Y., Gu, J., 2009. Numerical simulation of rock mass damage induced by underground explosion. Int. J. Rock Mech. Sci. 46, 1206–1213.
Xu, T., Yao, A., Zeng, X., Li, Y., 2011. Study on the security conditions of parallel laying Gas transmission pipeline under blast loading. ASCE, 1401–1411.
Yang, Y., Xie, X., Wang, R., 2010. Numerical simulation of operating metro tunnel induced by ground explosion. J. Rock Mech. Geotech. Eng. 2 (4), 373–384.
Zhang, S., Wang, G., Wang, C., Pang, B., Du, C., 2014. Numerical simulation of failure modes of concrete gravity dams subjected to underwater explosion. Eng. Fail. Anal. 36, 49–64.

freepaper.me FREE paper دانلود کننده مقالات علمی